

## Structure of boron nitride nanotubules

B. G. Demczyk,<sup>a),b)</sup> J. Cumings,<sup>b)</sup> and A. Zettl<sup>b)</sup>

*Department of Physics, University of California at Berkeley, Berkeley, California 94720*

R. O. Ritchie<sup>b)</sup>

*Department of Materials Science and Mineral Engineering University of California at Berkeley, Berkeley, California 94720*

(Received 10 November 2000; accepted for publication 1 March 2001)

We have used high-resolution transmission electron microscopy to resolve the [0001] projected basal plane structure and chirality relationships in boron nitride nanotubes. Evidence for tube growth along both  $\langle 10\bar{1}0 \rangle$  and  $\langle 11\bar{2}0 \rangle$  is found. Our results suggest that the  $\langle 11\bar{2}0 \rangle$  (armchair) tubes form first. Subsequent growth can take the form of a  $\langle 10\bar{1}0 \rangle$  (zig-zag) tube or additional armchair tubes. In both cases, the additional walls can be accommodated without the need for defect formation for circumferential tube closure. These results suggest that real boron nitride tubes may, in practice, realize their inherently high modulus and display less variation of mechanical properties than tubes comprised of carbon. © 2001 American Institute of Physics.  
[DOI: 10.1063/1.1367906]

Boron nitride (BN) nanotubes have been theoretically predicted<sup>1-3</sup> and experimentally observed<sup>4</sup> to have interesting mechanical and electrical properties. Although the crystalline nature of multiwall BN tubules has been demonstrated by transmission electron microscopy (TEM),<sup>5-13</sup> to this point a detailed examination of their structure has not been undertaken. We describe here results of high-resolution TEM characterization of these materials.

Nanotubes were synthesized via arc deposition, using a B-1 a/o Ni+1 a/o Co anode in a dynamically stabilized nitrogen atmosphere. Details of the synthesis were described previously.<sup>10</sup> BN-containing soot was collected from the deposition chamber walls. Samples were prepared for TEM examination by dispersing the soot in isopropanol via ultrasonic agitation, followed by deposition onto a holey carbon-coated 3 mm copper mesh grid. Specimens were examined in a Philips CM300 FEG TEM, operating at 300 kV. Digitized images were then analyzed by fast Hartley transform (FHT) techniques to reveal details of the local structure. All measurements taken from FHT patterns were made with reference to a standard bulk reference standard (GaN).

In agreement with previous TEM examination<sup>10</sup> of BN tubes synthesized by the same method, it was found that the majority of the tubules occurred in the form of two wall configurations. Figure 1 shows a TEM micrograph of such a structure. In this particular tube, the innermost tube diameter is  $\sim 2.1$  nm, consistent with earlier studies of similar tubes.<sup>10,13</sup> It should be noted, however, that in the present study other two-walled tubules were found with core diameters up to nearly 3 nm.

It is significant that we are able to resolve the atomic structure in the central region along portions of the tube. FHT analysis was utilized to obtain information on both the  $\{10\bar{1}0\}$  bilayer spacing and the chirality of the tube. In anal-

ogy to the carbon nanotube case,<sup>14</sup> this bilayer consists of B and N atoms arranged in alternating positions above and below an average position (Fig. 2). As the bilayer separation distance (0.067 nm) is below the line resolution of the instrument (0.10 nm), what is imaged in Fig. 1 is an “averaged out” plane of atoms. Therefore, the “hexagons” observed in the microscope appear to be rotated by  $30^\circ$  with respect to what actually exists in the structure. The FHT pattern for the two-wall tube is shown in Fig. 3(a). Due to the incomplete resolution of the central structure, only a portion of the expected six-fold pattern is obtained. The angle between the (0002) sidewall plane FHT maxima and those due to one of the bilayers, say  $\langle 10\bar{1}0 \rangle$ , is seen to be  $\sim 83^\circ$ . As in carbon nanotubes, there are two possible directions for the tube axis,  $\langle 10\bar{1}0 \rangle$  (“zig-zag” tubes) or  $\langle 11\bar{2}0 \rangle$  (“armchair” tubes). In an achiral tube with fiber axis along  $\langle 10\bar{1}0 \rangle$ , the maxima due

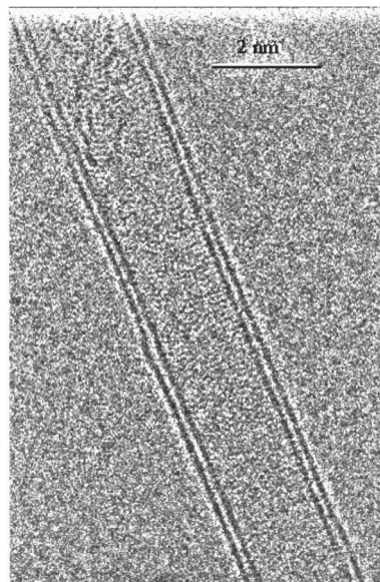


FIG. 1. Two-walled boron nitride tubule, with core structure partially resolved.

<sup>a)</sup>Electronic mail: demczyk@socrates.berkeley.edu

<sup>b)</sup>Also at Materials Sciences Division, Lawrence Berkeley National Laboratory, Berkeley, California 94720.

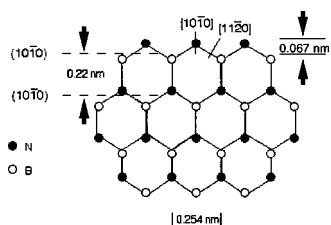


FIG. 2. Schematic sketch of boron nitride basal plane, showing the  $\{10\bar{1}0\}$  bilayers.

to the bilayer are orthogonal to the those due to the sidewalls.<sup>5</sup> If the fiber axis were  $\langle 11\bar{2}0 \rangle$ , the angle would be  $60^\circ$ . Any chirality in the tube would give rise to additional maxima symmetrically positioned across the orthogonal position. Close examination of Fig. 3(a) reveals that this is indeed the case. Hence, we conclude that this tube has an  $\sim 7^\circ$  chirality. Additional maxima arising from this same tube, due to  $(01\bar{1}0)$  and  $(1\bar{1}00)$ , for example, would be expected at  $37^\circ$  and  $19^\circ$  from the horizontal [the line joining the  $(0002)$  maxima]. Figure 4 depicts the expected diffraction pattern schematically. We are able to identify such reflections (within a few degrees) at  $39^\circ$  and  $19^\circ$  in Fig. 3(a).

Further examination of Fig. 3(a) reveals that other maxima, due to the second layer, appear at  $57^\circ$  and  $64^\circ$  and at  $\pm 4^\circ$  from the horizontal (the apparent maximum with a streak running through it at  $\sim 60^\circ$  is an artifact of the image processing, as careful examination reveals it not to lie on the same ‘‘circle’’ as the true maxima). A tube aligned along  $\langle 11\bar{2}0 \rangle$  would give rise to maxima at  $60^\circ$  and  $0^\circ$  to the horizontal. The  $4^\circ$  deviation from the expected positions could arise from chirality in the tube. Therefore, this two-walled tube consists of coaxial zig-zag ( $\langle 10\bar{1}0 \rangle$  fiber axis) and armchair ( $\langle 11\bar{2}0 \rangle$  fiber axis) tubes. Although it is not possible to determine from the direct experimental data which tube is innermost, arguments made below suggest that the armchair tube forms initially. This combination of two coaxial tubes with different crystallographic fiber axes explains the incomplete resolution of the  $[0001]$  projection in the tube center.

The bilayer spacing was found, from measurements on the FHT pattern, to be 0.22 nm. It should be noted that the maximum measurement error in this technique can be estimated at 5%, even though the systematic error in multiple measurements was less than 2%. Therefore, it can be reliably stated that the lattice spacing of the bilayer lies in the range of 0.21–0.23 nm. The  $(0002)$  sidewall spacing was found to be 0.37 nm, which is considerably larger than the expected  $\sim 0.33$  nm for boron nitride. It should be noted, however, that sidewall spacing variations (from an expected 0.34 nm

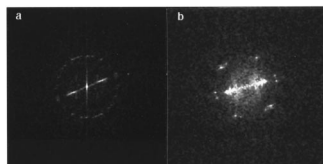


FIG. 3. FHT spectra of (a) Two-walled, (b) four-walled boron nitride nanotubes. Note orthogonal reflections in (a) and six-fold array in (b). Also note spacing difference in the  $(0002)$  reflections (innermost two maxima) between the two cases.

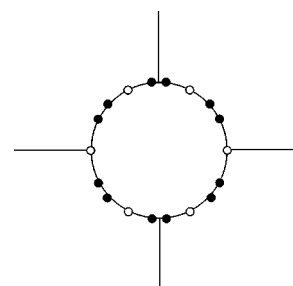


FIG. 4. Schematic diagram of diffraction pattern (FHT) expected for the two-walled boron nitride nanotube.

of this magnitude have been observed in multiwall carbon nanotubes,<sup>16</sup> where they were attributed to intertube repulsion. It should also be noted that no variation in the  $\{10\bar{1}0\}$  bilayer spacing was seen, nor did any noticeable tube structural degradation take place during the duration of the through-focal series of image exposures. Therefore, electron beam heating effects were not a factor. This sidewall spacing leads to an interesting geometrical argument, as will be described.

Although the majority of the tubules were of the two-walled variety, other forms were occasionally encountered. Figure 5 shows a four-walled tube in which the core structure is particularly well resolved. The FHT pattern [Fig. 3(b)] gives the full six-fold array of maxima from the  $\{10\bar{1}0\}$  bilayers comprising the core region. In this case, we observe a symmetrical splitting of all maxima. Analysis of the FHT pattern shows the fiber axis to be  $\langle 11\bar{2}0 \rangle$ , and that there is a small ( $\sim 4^\circ$ ) chirality present. It is interesting to note that this chirality is the same as was found for one of the two-walled tubes, aligned along this same direction. The nearly achiral alignment of all four tubes is evident from the excellent resolution of the core structure itself. In this case, we measured the  $(0002)$  and  $\{10\bar{1}0\}$  bilayer spacings as 0.34 and 0.22 nm, respectively.

The observation of near-zero chirality boron nitride nanotubes can be reconciled by considering the geometry involved in ‘‘rolling up’’ a sheet into a tube. For tubes aligned along  $\langle 10\bar{1}0 \rangle$  (zig-zag tubes), the ‘‘width’’ of a unit cell orthogonal to the tube axis is 0.254 nm (utilizing the

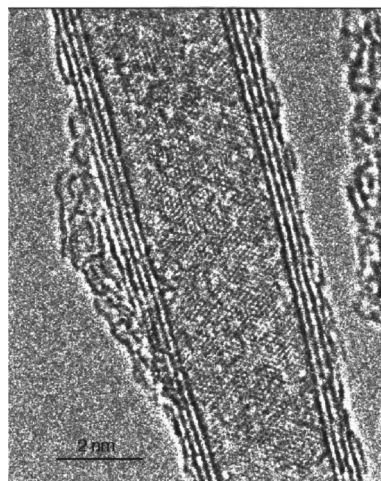


FIG. 5. Four-walled boron nitride tubule. Note particularly well resolved core structure, giving rise to six-fold array of atomic columns.

0.22 nm bilayer spacing determined as previously mentioned). Therefore, the circumference ( $2\pi \times 0.34$  nm) of a tube is not a precise multiple of 0.254 nm (= 8.4). However, if the (0002) spacing is allowed to “relax” to 0.37 nm (as just stated), this ratio becomes 9.15, much closer to an integer. Therefore, the strain due to the addition of tube layers can be accommodated without the need to introduce “interfacial dislocations.”<sup>15</sup> Consequently, an ABAB hexagonal stacking can be maintained throughout the structure. For tubes with an axis along  $\langle 11\bar{2}0 \rangle$ , the unit cell width becomes  $\sqrt{3} \times (0.254)$ . For our four-walled tube, with an (0002) spacing of 0.34 nm, the circumference/hexagon width ratio is 4.85, also not far from an integer. Since in both cases these tubes are inherently more defect-free, enhanced mechanical properties may be realized in practice.

It is of interest to speculate as to why  $\langle 11\bar{2}0 \rangle$  alignment prevails through all four layers in the four-walled tube, while the (apparently) outermost layer in the two-walled case aligns along  $\langle 10\bar{1}0 \rangle$ . Assuming that the  $\langle 11\bar{2}0 \rangle$  tube alignment is energetically favorable (as evidenced by the four-wall example), this observation suggests that the outer layer in the two-walled nanotube has realigned. In addition, since the same geometrical arguments can be made for pure carbon nanotubes, one may wonder why similar results have not been reported in carbon nanotubes, despite extensive study. In the BN case, the hexagons that comprise the nanotube layers consist of alternating B and N atoms (Fig. 2), which lead to a surface energy difference between zig-zag and armchair configurations. Since an atomic layer of B atoms is of considerably larger surface energy than one comprised of N atoms,<sup>17,18</sup> zig-zag tubes oriented such that N atoms form the top layer (assuming growth along the tube axis) are energetically favorable. These layers form alternately with the higher energy layers (B atom termination). In the armchair case, however, each additional surface layer added (comprised of an equal number of N and B atoms) is energetically equivalent. This constant energy growth mode is preferable to the “high-low” sequence involved in zig-zag tube growth. In the case of carbon nanotubes, since all atoms are identical, there is no *a priori* preference of tube growth direction.

It has been postulated<sup>10,19</sup> that BN nanotube growth terminates upon impingement with small metal catalyst clusters, or in flat-topped endcaps comprised of B–N bonds<sup>17,20</sup> (unlike the case of carbon nanotubes, which terminate in endcaps made up of polygons). Indeed, we have seen evidence for the former mechanism in the present work. We propose that upon growth termination the outermost tubule in a two-walled nanotube experiences a repulsive force due to the (smaller diameter) inner tube, giving rise to an intertube spacing greater than the  $\sim 0.33$  nm equilibrium spacing found in bulk BN. The outer BN tube then undergoes atomic rearrangement, resulting in alignment along  $\langle 10\bar{1}0 \rangle$ , to minimize the strain necessary to ensure tube closure. Such atomic rearrangements are plausible at the high growth temperatures ( $\geq 1000$  °C) involved. If the growth is not terminated at two layers, additional tubes can be added in the lower energy armchair configuration, with minimal straining necessary for tube closure. The outermost tubes in such cases experience less repulsive force from the innermost tubes and the equi-

librium BN interwall spacing is maintained. Therefore, the layers are “locked-in” to the armchair configuration. None of these processes would necessarily take place in carbon nanotubes, since the armchair configuration has no energetic advantage over zig-zag tubes.

The larger tube interwall spacing in two-walled BN nanotubes suggests that lower (than carbon nanotubes) friction “bearings,”<sup>21</sup> could be constructed from such structures.

The authors wish to note that subsequent to manuscript preparation, imaging of the central region of a three-walled BN nanotube, grown by chemical vapor deposition was reported.<sup>22</sup> The authors acknowledge this important contribution to the field.

The authors thank R. Sivamani for nanotube sample synthesis assistance and J. Wu for alloy preparation. TEM was performed at the National Center for Electron Microscopy at the Lawrence Berkeley National Laboratory. This research was supported in part by the Director of the Office of Energy Research, Office of Basic Energy Sciences, Materials Sciences Division of the United States Department of Energy, Contract No. DEAC03-76SF00098 and Grant Nos. DMR 98-01738 and DMR 95-01156 from the National Science Foundation.

- <sup>1</sup>A. Rubio, J. Corkill, and M. L. Cohen, *Phys. Rev. B* **49**, 5081 (1994).
- <sup>2</sup>X. Blase, A. Rubio, S. G. Louie, and M. L. Cohen, *Europhys. Lett.* **28**, 335 (1994).
- <sup>3</sup>E. Hernandez, C. Goze, P. Bernier, and A. Rubio, *Phys. Rev. Lett.* **80**, 4502 (1998).
- <sup>4</sup>N. G. Chopra and A. Zettl, *Solid State Commun.* **105**, 297 (1998).
- <sup>5</sup>R. Tenece, L. Margulus, M. Genut, and G. Hodes, *Nature (London)* **360**, 444 (1992).
- <sup>6</sup>D. Golberg, Y. Bando, M. Eremets, K. Takemura, K. Kurashima, and H. Yusa, *Appl. Phys. Lett.* **69**, 2045 (1996).
- <sup>7</sup>D. P. Yu, X. S. Sun, C. S. Lee, I. Bello, S. T. Lee, H. D. Gu, K. M. Leung, G. W. Zhou, Z. F. Dong, and Z. Zhang, *Appl. Phys. Lett.* **72**, 1966 (1998).
- <sup>8</sup>G. W. Zhou, Z. Zhang, Z. G. Bai, and D. P. Yu, *Solid State Commun.* **109**, 555 (1999).
- <sup>9</sup>Z. Weng-Sieh, K. Cherrey, N. G. Chopra, X. Blase, Y. Miyamoto, A. Rubio, M. L. Cohen, S. G. Louie, A. Zettl, and R. Gronsky, *Phys. Rev. B* **51**, 11229 (1995).
- <sup>10</sup>N. G. Chopra, R. J. Luyken, K. Cherrey, V. H. Crespi, M. L. Cohen, S. G. Louie, and A. Zettl, *Science* **269**, 966 (1995).
- <sup>11</sup>O. Stephen, P. M. Ajayan, C. Colliex, P. Redlich, J. M. Lambert, P. Bernier, and P. Lefin, *Science* **266**, 1683 (1996).
- <sup>12</sup>A. Loiseau, F. Willaime, N. Demoncey, G. Hug, and H. Pascard, *Phys. Rev. Lett.* **76**, 4737 (1996).
- <sup>13</sup>J. Cumings and A. Zettl, *Chem. Phys. Lett.* **316**, 211 (2000).
- <sup>14</sup>M. Bretz, B. G. Demczyk, and L. Zhang, *J. Cryst. Growth* **141**, 304 (1994).
- <sup>15</sup>X. F. Zhang, X. B. Zhang, G. Van Tendeloo, S. Amelinckx, M. Op de Beeck, and J. Van Landuyt, *J. Cryst. Growth* **130**, 368 (1993).
- <sup>16</sup>C.-H. Kiang, M. Endo, P. M. Ajayan, G. Dresselhaus, and M. S. Dresselhaus, *Phys. Rev. Lett.* **81**, 1869 (1998).
- <sup>17</sup>M. Terrones, W. K. Hsu, H. Terrones, J. P. Zhang, S. Ramos, J. P. Hare, R. Castillo, K. Prassides, A. K. Cheetham, H. W. Kroto, and D. R. M. Walton, *Chem. Phys. Lett.* **259**, 568 (1996).
- <sup>18</sup>A. Zangwill, *Physics at Surfaces* (Cambridge University Press, Cambridge, UK, 1989), p. 11.
- <sup>19</sup>N. G. Chopra and A. Zettl, in *Fullerines, Chemistry, Physics and Technology*, edited by K. M. Kadish and R. S. Ruoff (Wiley, New York, 2000), pp. 767–794.
- <sup>20</sup>A. Loiseau, F. Willaime, N. Demoncey, C. Hug, and H. Pascand, *Phys. Rev. Lett.* **76**, 4737 (1996).
- <sup>21</sup>J. Cumings and A. Zettl, *Science* **289**, 602 (2000).
- <sup>22</sup>D. Goldberg, Y. Bando, L. Bourgeois, K. Kurashima, and T. Sato, *Appl. Phys. Lett.* **77**, 13 (2000).